


# Arpin is critical for phagocytosis in macrophages and is targeted by human rhinovirus

Jamil Jubrail<sup>1</sup>, Kshanti Africano-Gomez<sup>1,†</sup>, Floriane Herit<sup>1,†</sup>, Anna Mularski<sup>1</sup>, Pierre Bourdoncle<sup>1</sup>, Lisa Oberg<sup>2</sup>, Elisabeth Israelsson<sup>2</sup>, Pierre-Regis Burgel<sup>1,3</sup>, Gaell Mayer<sup>4</sup>, Danen M Cunoosamy<sup>2</sup>, Nisha Kurian<sup>5</sup> & Florence Niedergang<sup>1,\*</sup> 

## Abstract

Human rhinovirus is a causative agent of severe exacerbations of chronic obstructive pulmonary disease (COPD). COPD is characterised by an increased number of alveolar macrophages with diminished phagocytic functions, but how rhinovirus infection affects macrophage function is still unknown. Here, we describe that human rhinovirus 16 impairs bacterial uptake and receptor-mediated phagocytosis in macrophages. The stalled phagocytic cups contain accumulated F-actin. Interestingly, we find that human rhinovirus 16 downregulates the expression of Arpin, a negative regulator of the Arp2/3 complex. Importantly, re-expression of the protein rescues defective internalisation in human rhinovirus 16-treated cells, demonstrating that Arpin is a key factor targeted to impair phagocytosis. We further show that Arpin is required for efficient uptake of multiple targets, for F-actin cup formation and for successful phagosome completion in macrophages. Interestingly, Arpin is recruited to sites of membrane extension and phagosome closure. Thus, we identify Arpin as a central actin regulator during phagocytosis that it is targeted by human rhinovirus 16, allowing the virus to perturb bacterial internalisation and phagocytosis in macrophages.

**Keywords** actin; Arp2/3; bacteria; Macrophage; phagosome

**Subject Categories** Immunology; Membranes & Trafficking; Microbiology, Virology & Host Pathogen Interaction

**DOI** 10.15252/embr.201947963 | Received 20 February 2019 | Revised 9 October 2019 | Accepted 19 October 2019 | Published online 13 November 2019

**EMBO Reports (2020) 21: e47963**

## Introduction

Human rhinovirus (HRV) belongs to the *Picornaviridae* family. It is a small, non-enveloped virus with a single-stranded, positive-sense

RNA genome encased within an icosahedral protein capsid with 60 copies each of four key viral proteins, VP1–VP4 [1]. Dependent on the clades, the viruses use either the low-density lipoprotein receptor (LDLR) family, the intracellular adhesion molecular 1 (ICAM1) or cadherin-related family member 3 to bind and enter cells [2–5]. HRV is known to productively infect epithelial cells [6–12], but the response in macrophages has received limited attention [7,13]. Reports suggest that HRV can infect monocytes/macrophages [7,14,15]. A recent study demonstrated that epithelial cells directly enhance the replication of rhinovirus in monocytes [15]. Traditionally, HRV is seen as an upper respiratory tract pathogen [16]. However, mounting evidence shows that HRV can infect the lower respiratory tract in patients with chronic inflammatory diseases including chronic obstructive pulmonary disease (COPD) driving disease exacerbations [17–20]. Interestingly, in subjects experimentally infected with RV16, RV was ingested by recruited CD68-positive and CD11b-positive macrophages in asthmatic humans, providing direct evidence that tissue macrophages in the lower airways contribute to anti-RV responses *in vivo* [21]. How HRV disrupts macrophage/monocyte functions remains unknown, but HRV was reported to induce a defective secondary response in macrophages [13,22–24].

An important arm of the innate immune responses is the phagocytic uptake by myeloid cells. Phagocytosis is a mechanism of internalisation of large particulate material, cell debris and microorganisms [25–27]. It is strictly dependent on actin polymerisation that represents the major force driving plasma membrane deformation and engulfment. Actin polymerisation is induced by surface phagocytic receptors after ligation of the target and intracellular signal transduction. Phagocytic receptors include receptors for host serum factors (opsonins) such as immunoglobulin (Ig) and the complement fragment C3bi that engage Fc receptor (FcRs) and complement receptors (CR3,  $\alpha$ M $\beta$ 2), respectively, and non-opsonic receptors such as the Toll-like receptors (TLRs), the lectins and scavenger receptors [27–29]. Key players of the signalling to actin polymerisation are the small GTPases of the Rho family [30,31]. In the well-characterised

<sup>1</sup> Université de Paris, Institut Cochin, INSERM, U1016, CNRS, UMR 8104, Paris, France

<sup>2</sup> Translational Science and Experimental Medicine, Research and Early Development, Respiratory Inflammation and Autoimmunity, BioPharmaceuticals R&D, AstraZeneca, Gothenburg, Sweden

<sup>3</sup> Department of Pneumology, Hospital Cochin, AP-HP, Paris, France

<sup>4</sup> Late-stage development, Respiratory, Inflammation and Autoimmunity (RIA), BioPharmaceuticals R&D, AstraZeneca, Gothenburg, Sweden

<sup>5</sup> Respiratory Inflammation and Autoimmune Precision Medicine Unit, Precision Medicine, Oncology R&D, AstraZeneca, Gothenburg, Sweden

\*Corresponding author. Tel: +33 6753 23892; E-mail: florence.niedergang@inserm.fr

<sup>†</sup>These authors contributed equally to this work

FcR-mediated phagocytosis, Cdc42 activation in the nascent phagocytic cup activates effectors like N-WASP, an actin nucleation-promoting factor (NPF) that acts on the actin-related protein 2/3 (Arp2/3) actin nucleation complex. Rac1 is then essential for F-actin polymerisation to complete extension and closure, through activation of another NPF, the WAVE complex [26,32,33].

During phagosome formation, actin polymerisation is transient and forms a specific F-actin ring-like structure, called the phagocytic cup. The actin ring diameter progressively shrinks until the membrane extensions eventually fuse, a step promoted by dynamin [26,34]. Actin filaments experience a high turnover, with intense polymerisation in the tips of the membrane folds and depolymerisation at the base of the phagocytic cup [33,35–38]. Several protein activities have been reported to play a role in actin remodelling, including cofilin and enzymatic activities leading to PIP(4,5)<sub>2</sub> hydrolysis or consumption [36,38–42].

In addition, proteins inhibiting directly Arp2/3 have been described, namely Gadkin, PICK1 and Arpin [43–45], for which no role in phagocytosis has been reported yet. These inhibitors are not found freely in the cytosol but localise to specific membranes like NPFs making them ideal candidates to counteract NPF activity [46]. Arpin was found to bind to the Arp2/3 complex without activating it [45]. Instead, Arpin exposes its COOH terminal acidic tail to inhibit the Arp2/3 complex [47,48]. In cells studied so far, Arpin localises at lamellipodial edges along with the WAVE complex [45]. The ability of Arpin to interact with Arp2/3 was found to depend on Rac1 signalling [45]. In response to Rac1 signalling, Arpin inhibited Arp2/3 at lamellipodial tips where Rac1 also stimulates actin polymerisation through WAVE [45]. This placed Arpin downstream of Rac1 in a cycle with Rac inducing and inhibiting actin polymerisation [45]. The major function of Arpin described to date is the inhibition of cell migration [49] and a control of cell steering [45].

In this study, we demonstrate that HRV16 impairs macrophage phagocytosis of multiple targets. We report that HRV16 induced a downregulation of Arpin in macrophages. By re-expressing Arpin in a model cellular system where HRV16 exposure led to decreased internalisation, we could rescue this defect. Further analysis revealed that Arpin is required for efficient internalisation. Thus, Arpin plays a critical role in coordinating and orchestrating actin remodelling around internalised particles, necessary for efficient phagocytosis. Therefore, we add phagocytosis to the growing list of functions being attributed to Arpin and highlight a host cell factor specifically targeted by rhinovirus.

## Results

### Human rhinovirus 16 impairs bacterial internalisation in human macrophages

We used HRV16 for our studies because it is commonly isolated in COPD [19,20]. We first set out to determine whether macrophages could internalise bacteria after HRV16 challenge. We challenged human monocyte-derived macrophages (hMDMs) with HRV16, HRV16 inactivated by a UV treatment (HRV16<sup>UV</sup>) or mock-infected medium (MI) for 1 h at room temperature followed by overnight rest. The next day, we exposed them to non-typeable *Haemophilus influenzae* (NTHi), *Moraxella catarrhalis*, *Staphylococcus aureus* or

*Pseudomonas aeruginosa* that are frequently associated with exacerbations of COPD [20]. We measured internalisation at 30 and 120 min after washing and incubation with antibiotics to kill extracellular bacteria. We found that hMDMs challenged with HRV16 were significantly impaired in their ability to internalise all four bacteria over 120 min compared to hMDMs challenged with HRV16<sup>UV</sup> or mock-infected (Fig 1A–D). To determine whether this result was due to a high HRV16 tissue culture infective dose 50 (TCID<sub>50</sub>), we repeated our experiments over a range of TCID<sub>50</sub>'s and measured internalisation of NTHi and *S. aureus* over 120 min. We found that HRV16 impaired the internalisation of NTHi (Fig EV1A–E) and *S. aureus* in hMDMs (Fig EV2A–E) from TCID<sub>50</sub>'s as low as  $1 \times 10^3$  reaching a maximal impairment at TCID<sub>50</sub>  $1 \times 10^7$ . We also calculated the percentage inhibition of internalisation of NTHi or *S. aureus* at 120 min for all TCID<sub>50</sub>'s relative to mock infection and found that on average the impairment in internalisation caused by HRV16 was greater for *S. aureus* than NTHi at TCID<sub>50</sub>  $1 \times 10^5$  or  $1 \times 10^6$  but identical and maximal by TCID<sub>50</sub>  $1 \times 10^7$  reaching 80% (Figs EV1F and EV2F).

Then, because reduced internalisation of bacteria could be due to a reduced initial binding to the cell surface, we repeated our experiments over 30 min by incubating hMDMs with the different bacteria on ice for 5, 15 or 30 min (Fig 1E–H). No differences in bacterial attachment to hMDMs were observed in cells challenged with HRV16 or control conditions. These results indicated that HRV16 impaired the response of hMDMs to bacteria at the level of internalisation.

Finally, because HRV16 is a predominant cause of exacerbation in COPD [20,50], we decided to explore the effect of HRV16 challenge on bacterial internalisation by human alveolar macrophages (AMs) (Table 1). We found that non-smoker, non-COPD AMs challenged with HRV16 were significantly impaired in their ability to internalise NTHi over 120 min compared to AMs challenged with HRV16<sup>UV</sup> or mock infection (MI) (Fig 1I). When we repeated our experiments using healthy smoker AMs, we first found that they internalised less bacteria at baseline relative to non-smoker, non-COPD AMs (Fig 1J). Interestingly, even if smoking itself impaired bacterial internalisation, HRV16 challenge led to an additive impairment in NTHi internalisation by healthy smoker AMs (Fig 1J).

Taken together, these results demonstrate that HRV16 challenge in *in vitro* derived macrophages impaired their ability to internalise bacteria. Importantly, we observed the same defect in human lung macrophages.

### Human rhinovirus 16 impairs zymosan, CR3- and FcR-mediated internalisation in human macrophages

We next wanted to determine whether the impairment in internalisation caused by HRV16 was specific to bacteria. Therefore, we exposed hMDMs post-HRV16 challenge to zymosan for 60 min. We found that hMDMs challenged with HRV16 were significantly impaired in their ability to internalise zymosan compared to MI or HRV16<sup>UV</sup>-treated hMDMs (Fig 2A), internalising on average 70% less zymosan (Fig 2A). To allow us to better characterise the defect in internalisation caused by HRV16, we decided to next analyse the internalisation of opsonised particles that trigger only one type of phagocytic receptor. Therefore, post-HRV16 challenge we exposed hMDMs to sheep red blood cells (SRBC) opsonised with either IgM-iC3b or IgG for 60 min. hMDMs challenged with HRV16 were

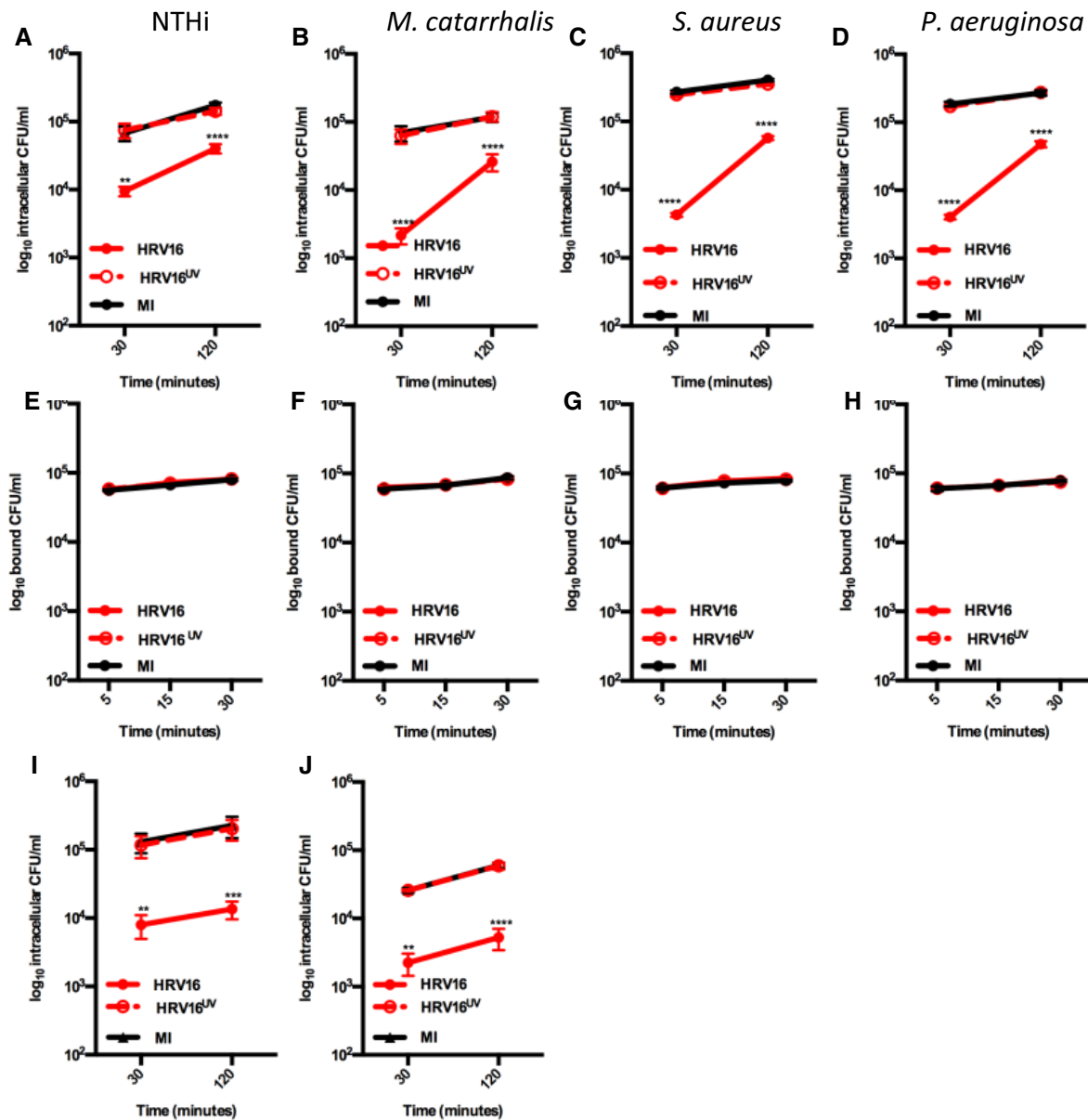


**Figure 1. HRV16 impairs bacterial internalisation by macrophages.**

A–H hMDMs were challenged with HRV16, HRV16<sup>UV</sup> or MI and then exposed to either (A, E) NTHi, (B, F) *Moraxella catarrhalis*, (C, G) *Staphylococcus aureus* or (D, H) *Pseudomonas aeruginosa* to assess internalisation (A–D) or binding (E–H). *n* = 3 biological replicates on different donors \*\**P* < 0.01, \*\*\*\**P* < 0.0001 two-way ANOVA with Dunnett’s post-test vs. MI.

I, J (I) Non-smoker, non-COPD or (J) healthy smoker, non-COPD AM were challenged with HRV16 or controls and then exposed to NTHi to assess internalisation. *n* = 4 biological replicates on different donors \*\**P* < 0.01, \*\*\**P* < 0.001, \*\*\*\**P* < 0.0001 two-way ANOVA with Dunnett’s post-test vs. MI.

Data information: Error bars represent standard error of the mean (SEM).

significantly impaired in their ability to internalise either IgM-iC3b- or IgG-opsonised SRBC compared to control or HRV16<sup>UV</sup>-treated hMDMs (Fig 2B–E), internalising on average 50% less of either

**Table 1. Patient demographics for AM samples used in Fig 1.**

	Non-smoker	Healthy smoker
Male/female	3/1	3/1
Age	44 (average)	46 (average)
Ex/current smoker	N/A	0/4

particle (Figs 2B and C, and EV3A showing the internalisation index). Representative images of mock-infected or HRV16-treated hMDMs are shown in Fig 2D and E, highlighting the internalised SRBC in green. The images clearly demonstrate the impaired internalisation caused by HRV16 towards IgM-iC3b-opsonised SRBC (Fig 2D) or IgG-opsonised SRBC (Fig 2E).

These results along with the results in Fig 1 demonstrate that HRV16 challenge of hMDMs impairs various phagocytic pathways, suggesting that HRV16 targets a global regulator of phagocytosis in macrophages.

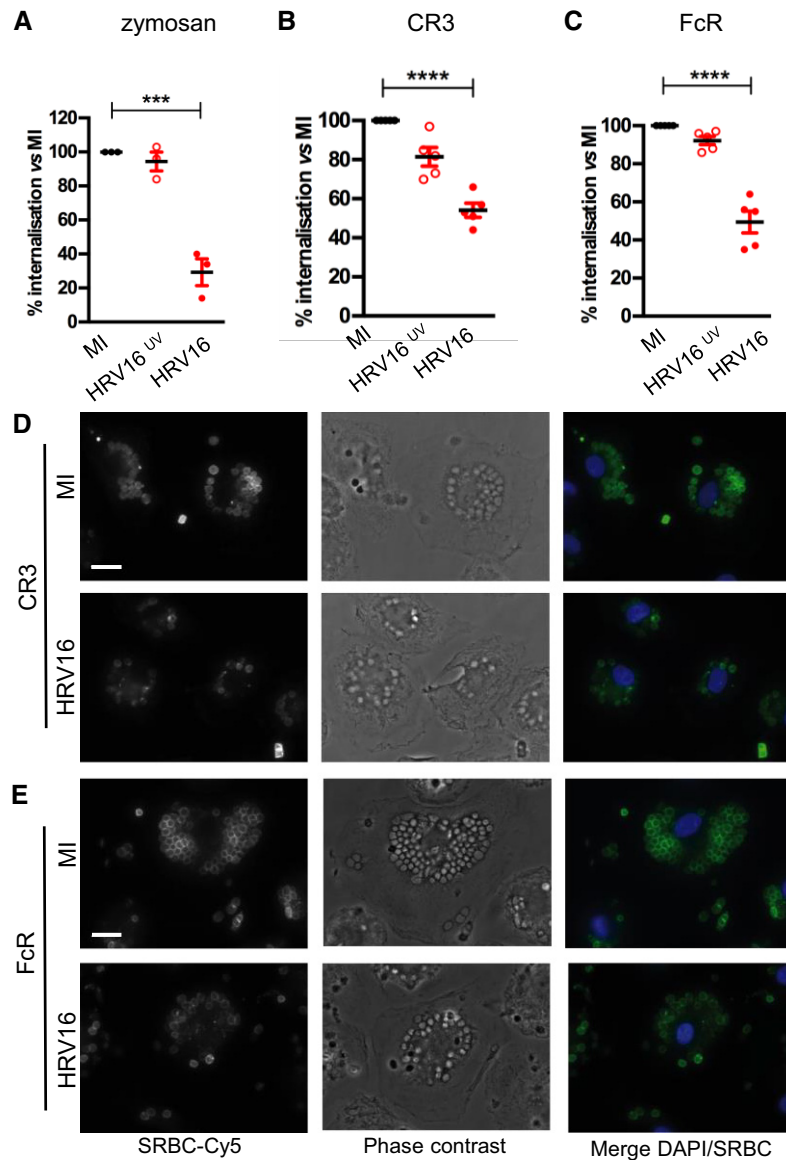


**Figure 2. HRV16 impairs receptor-mediated internalisation by macrophages.**

A–C hMDMs were challenged with HRV16 or controls and then exposed to (A) zymosan for 60 min,  $n = 3$  donors, 30 random cells/coverlip; (B) IgM-ic3b-opsonised SRBC for 60 min,  $n = 5$  donors, 30 random cells/coverlip; or (C) IgG-opsonised SRBC for 60 min,  $n = 5$  donors, 30 random cells/coverlip.  $***P < 0.001$ ,  $****P < 0.0001$  one-way ANOVA with Bonferroni's post-test vs. MI. Error bars represent standard error of the mean (SEM).  
 D Representative images of MI or HRV16-challenged hMDMs at 60 min post-IgM-ic3b SRBC internalisation. Intracellular particles are labelled with Cy5-coupled F(ab)<sub>2</sub> anti-rabbit Ig and DAPI. Scale bar, 15  $\mu$ m.  
 E Representative images of MI or HRV16-challenged hMDMs at 60 min post-IgG-SRBC. Intracellular particles are labelled with Cy5-coupled F(ab)<sub>2</sub> anti-rabbit Ig and DAPI. Scale bar, 15  $\mu$ m.

### Human rhinovirus 16 impairs phagocytic cup formation in human macrophages

Having shown that HRV16 impaired internalisation by hMDMs, we next set out to analyse whether HRV16 altered membrane remodelling at the onset of phagocytosis. For this, we challenged hMDMs with HRV16 or MI control and then exposed them to IgG-opsonised SRBC for 2–30 min. The samples were stained with phalloidin to analyse F-actin recruitment around the internalised SRBC (Fig 3A, Z projections of stack images). We counted the number of F-actin-

positive cups (Fig 3B) and calculated the enrichment of F-actin around the SRBC at each phagocytic cup relative to the cell cortex [51] (Fig 3C). Over the first 5 min of internalisation, we did not observe any significant difference in the number of F-actin cups that formed in mock-infected or HRV16-treated hMDMs (Fig 3B). Despite this, there was less internalisation in HRV16-challenged hMDMs over the first 5 min compared to control hMDMs (Fig 3D). Importantly, there was no equivalent difference in SRBC association with HRV16-challenged hMDMs over these first 5 min (Fig 3E). Despite the similarity in the number of F-actin cups that formed at 5 min in

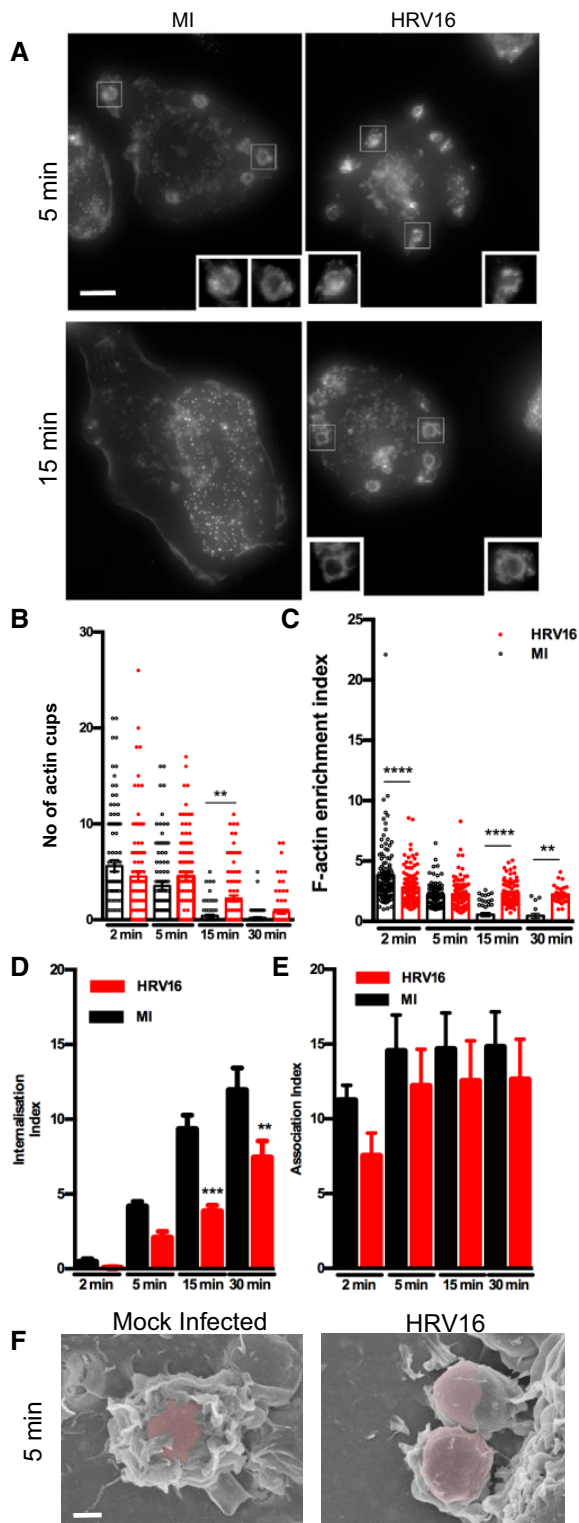


**Figure 3. HRV16 impairs phagocytic cup extension.** hMDMs were challenged with HRV16 or MI and then exposed to IgG-opsonised SRBC for 2–30 min.

**A** Representative images of a Z projection of phalloidin staining at 5 and 15 min post-internalisation in MI and HRV16-challenged hMDMs. Scale bar, 15  $\mu$ m.

**B** Quantification of the number of actin cups in hMDMs,  $n = 3$  donors, at least 80 cups at the early time points and 8–80 cups at later time points depending on the time.

**C** Quantification of the initial F-actin enrichment around internalised particles in hMDMs, on  $n = 3$  different donors.

**D** Quantification of internalisation of SRBC over 30 min,  $n = 3$  donors, 30 random cells/cover slip.

**E** Quantification of association of SRBC to hMDMs,  $n = 3$  donors, 30 random cells/cover slip.

**F** Scanning electron microscopy images after 5 min of contact with IgG-opsonised SRBC showing differences in cup formation. Scale bar, 1  $\mu$ m.

Data information:  $**P < 0.01$ ,  $***P < 0.001$ ,  $****P < 0.0001$  one-way ANOVA with Bonferonni's post-test vs. MI. Error bars represent standard error of the mean (SEM).

both conditions, we could observe differences in the F-actin make up around the internalised SRBC. The cups looked thinner and less defined in HRV16-challenged hMDMs compared to control hMDMs, and the intensity of F-actin staining around the cups was lower in the early time point (2 min, Fig 3C). At 15 and 30 min

post-internalisation, we observed a sustained number of F-actin cups in HRV16-challenged hMDMs compared to mock-infected hMDMs where only few F-actin cups were still observed (Fig 3B) and this reached statistical significance at 15 min (Fig 3B). In line with these results, we observed significantly less internalisation over these later time points in HRV16-challenged hMDMs (Fig 3D), with no differences in association (Fig 3E). Importantly, internalisation was still inhibited at 60 min in HRV16-challenged hMDMs, demonstrating that HRV16 does not just delay, but inhibits, internalisation (Fig EV3A). When we next looked at F-actin cups at 15 min, we could see they were stalled and still contained F-actin, similar to MI at 5 min, but the intensity of staining was lower (Fig 3A and C). Very interestingly, as opposed to the control cells where the cups had disassembled and only adhesion structures were detected in the images projected in Z, we observed a sustained enrichment of F-actin around internalised SRBC that was similar from 5 to 30 min and showed no clear decrease (Fig 3A and E).

Finally, to better visualise the membrane architecture in HRV16-challenged hMDMs, we performed scanning electron microscopy on mock-infected or HRV16-challenged hMDMs after 5 min of internalisation of IgG-opsonised SRBC (Fig 3F). In mock-infected hMDMs, we often observed a lot of membrane folds in several layers progressing over the SRBC (Fig 3F). In HRV16-challenged hMDMs, there were fewer membrane folds, and the membrane covering the SRBC was thinner and only partially covered of the SRBC (Fig 3F). Combined with our fluorescence images, these results demonstrate that HRV16 impairs internalisation in hMDMs by perturbing early phagosome formation and actin remodelling.

**Human rhinovirus does not affect the expression of F-actin in human macrophages but downregulates the expression of Arpin**

We next set out to determine more precisely whether HRV16 disrupted the actin cytoskeleton in hMDMs. We challenged hMDMs with HRV16 or control medium for 1 h followed by overnight rest and then stained the cells with phalloidin. The F-actin network did not appear to be disrupted by HRV16, but the global F-actin intensity was lower in HRV16-challenged hMDMs compared to mock-infected hMDMs (Fig 4A). When we quantified our images, we first



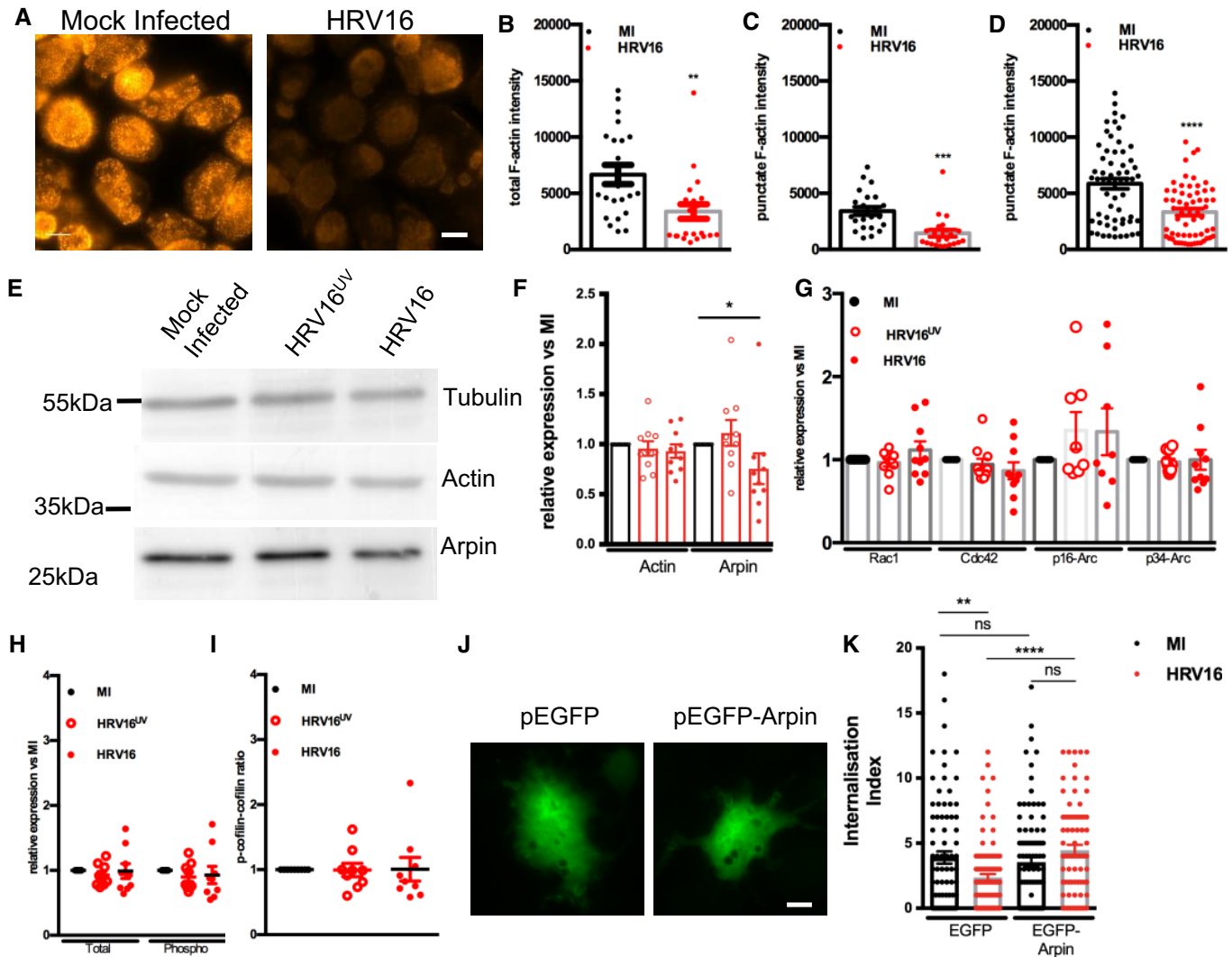


**Figure 4. HRV16 downregulates Arpin expression in macrophages.**

hMDMs were challenged with HRV16 or controls and then stained or lysed.

A Representative images of MI or HRV16-challenged hMDMs stained with phalloidin-Cy3 at 24 h post-infection. Scale bar, 15  $\mu$ m.

B Quantification of the total F-actin intensity per field,  $n = 3$  donors, 20 random fields per coverslip

C Quantification of the punctate F-actin intensity per field,  $n = 3$  donors, 20 random fields per coverslip.

D Quantification of the punctate F-actin intensity per cell in 20 cells per donor per condition,  $n = 3$  different donors.

E Immunoblot of lysates from hMDMs challenged with MI, HRV16<sup>UV</sup> or HRV16 to detect Arpin or actin.

F Quantification of immunoblots normalised to MI control,  $n = 10$  experiments on different donors.

G Quantification of Rac1, Cdc42, p16-Arc, and p34-Arc,  $n = 10$  experiments on different donors.

H Quantification of total and phosphorylated cofilin expression,  $n = 9$  experiments on different donors.

I Relative activation of cofilin vs. total cofilin,  $n = 9$  experiments on different donors.

J RPE-1-Fc $\gamma$ RIIA cells challenged with mock medium (MI) and transfected with plasmids encoding EGFP (left) or EGFP-Arpin (right).

K Quantification of FcR phagocytosis in RPE-1-Fc $\gamma$ RIIA cells challenged with mock medium (MI) or HRV16 and then transfected to express EGFP or EGFP-Arpin,  $n = 4$  experiments, between 30 and 50 random cells.

Data information: In (B–D),  $***P < 0.01$ ,  $****P < 0.0001$  paired t-test vs. MI. In (F),  $*P < 0.05$  one-way ANOVA with Bonferonni's post-test vs. MI. In (K),  $**P < 0.01$ ,  $****P < 0.0001$  unpaired t-test. Error bars represent standard error of the mean (SEM).

Source data are available online for this figure.

determined that the total F-actin intensity in each field imaged was significantly lower in HRV16-challenged hMDMs compared to control hMDMs (Fig 4B). In addition, we observed that the intensity of the punctate F-actin was significantly lower in HRV16-challenged vs. mock-treated hMDMs (Fig 4C). Because the primary cells are

heterogeneous, we also analysed the data in Fig 4C on a per-cell basis and determined that the intensity of staining of punctate F-actin was significantly lower in individual cells in HRV16-challenged hMDMs compared to control conditions (Fig 4D). Collectively, these results suggested that HRV16 disrupts the F-actin network in hMDMs.

We therefore postulated that there might be globally less actin protein in our HRV16-challenged hMDMs. However, immunoblot analysis revealed no significant change in the actin expression between HRV16-challenged (lane 3), HRV16<sup>UV</sup>-challenged (lane 2) or mock-infected cells (lane 1) (Fig 4E and F). Although the quantification across 10 donors revealed variations in the global amount, there was no significant trend in either direction towards more or less actin in either condition (Fig 4F). This result suggested that HRV16 might be targeting a regulator of the F-actin network in hMDMs rather than the G-actin pool. To test this hypothesis, we challenged hMDMs to HRV16 or HRV16<sup>UV</sup> or mock conditions and screened for a range of actin-associated proteins. Of the actin regulators that we tested, we found that the Arp2/3 inhibitor Arpin was consistently and significantly downregulated on average by 30% in HRV16-challenged hMDMs compared to control conditions (Fig 4E–G). Of note, there was no effect on the global expression of Rac1, which is upstream of Arpin and activates Arp2/3 via WAVE [52] (Fig 4G). We found no significant decrease in the expression of Cdc42 that activates Arp2/3 via WASP (Fig 4G). We then looked at subunits of Arp2/3 including ArpC2 (p34-Arc) and ArpC5 (p16-Arc). We observed no difference in the global expression of p34-Arc in HRV16-challenged hMDMs compared to control conditions and a non-significant increase in the global expression of p16-Arc that was not specific to the live virus (Fig 4G). We also analysed the expression of cofilin and observed no difference in the total or phosphorylated forms (Fig 4H and I, ratio).

Finally, to further confirm that the disruption of Arpin expression by HRV16 was mediating deficient internalisation caused by HRV16, we set out to re-express the protein and analyse whether internalisation is restored. To overcome the issues of transfecting primary human macrophages, we made use of retinal pigment epithelial-1 (RPE-1) cells that were transduced with lentivirus to express the phagocytic FcγRIIA/CD32. We first verified by flow cytometry that the transduced cells expressed the receptor and found that 100% of cells were positive for CD32 (Fig EV4A). The RPE-1-FcγRIIA cells were able to specifically phagocytose IgG-opsonised SRBC as compared with non-opsonised particles, while the parental cells were not competent for this phagocytosis (Fig EV4B–D). Next, we exposed these cells to HRV16 or to mock-infected medium for 1 h followed by overnight rest and then challenged them with IgG-opsonised SRBC for 1 h. We found that RPE-1-FcγRIIA cells exposed to HRV16 internalised on average 40% less SRBC compared to a mock treatment (Fig EV4D). Having confirmed that RPE-1-FcγRIIA cells responded like human macrophages to HRV16, we exposed these cells to HRV16 or mock medium and, after the overnight rest, transfected them with plasmids encoding either EGFP or EGFP-Arpin for 24 h (Fig 4J and K). Then, we performed a phagocytosis experiment using IgG-opsonised SRBC for 1 h. We demonstrated that RPE-1-FcγRIIA cells exposed to HRV16 and then transfected with EGFP internalised significantly fewer SRBC compared to mock infection controls, which averaged an approximate 40% decrease (Fig 4K). Importantly, when RPE-1-FcγRIIA cells were exposed to HRV16 and then transfected to express EGFP-Arpin, the efficiency of internalisation of SRBC was restored (Fig 4K).

Taken together, our results show that live HRV16 impairs the F-actin network in hMDMs and reveal that the Arp2/3 inhibitor Arpin is downregulated in live HRV16-treated macrophages. Furthermore, these results demonstrate that HRV16 specifically targeted Arpin to

decrease internalisation and that transient expression of the protein restored the phagocytic capacities of HRV16-treated cells. Therefore, Arpin is a crucial factor targeted by this rhinovirus to impair phagocytosis.

### Arpin knockdown impairs bacterial internalisation

Because the Arp2/3 inhibitor had never been implicated in phagocytosis, we next addressed whether a decrease in Arpin expression could recapitulate the perturbations in phagosome formation that we observed in macrophages challenged with HRV. We treated hMDMs with two siRNA against Arpin [45] or luciferase as a control, or left them non-treated for 96 h. Immunoblot analysis and quantification demonstrated significant Arpin reduction for both siRNA sequences in 9 donors (Fig 5A and B). We then challenged the Arpin-depleted macrophages with either NTHi, *M. catarrhalis*, *S. aureus* or *P. aeruginosa* for up to 120 min. We found that hMDMs treated with Arpin siRNA were significantly impaired in their ability to internalise all bacteria (Fig 5C–F) relative to non-treated hMDMs. Importantly, hMDMs treated with siLuciferase demonstrated similar bacterial internalisation to non-treated hMDMs (Fig 5C–F). Finally, we also assessed bacterial binding to hMDMs over 5–30 min of infection post-siRNA treatment and found no difference between the four conditions (Fig EV5A–D). These results demonstrate that Arpin plays a crucial role in bacterial internalisation in hMDMs.

### Arpin knockdown impairs membrane extension around internalised particles

Having shown that Arpin knockdown impaired internalisation of bacteria by human macrophages, we next set out to analyse whether it impaired F-actin dynamics at the phagocytic cup. We treated hMDMs with Arpin siRNA or controls and after 96 h challenged them with IgG-opsonised SRBC for 15–30 min (Fig 6A–D). Significantly fewer SRBC were internalised in macrophages when Arpin was knocked down, as compared with control conditions (Fig 6B). In contrast, there was a non-significant trend towards less association of SRBC to hMDMs treated with siRNA against Arpin (Fig 6C), indicating that depletion of Arpin leads to a defective phagocytosis. Similar to what we observed with HRV16, internalisation was not simply delayed in Arpin-depleted macrophages, as internalisation was still impaired after 60 min (Fig EV3B). In addition, we observed significantly more F-actin cups in Arpin-depleted macrophages as compared to control conditions at 15 min post-internalisation (Fig 6A and D). We then examined the F-actin cups in Arpin-depleted vs. non-treated or siLuciferase-treated hMDMs where the F-actin cups were complete, with homogeneous F-actin organisation around the particles (Fig 6A). In contrast, Arpin knockdown not only led to an increased number of cups visible in Fig 6A, but also to cups that appeared fragmented with puncta of staining (Fig 6A). By 30 min post-internalisation, there were very few cups in control conditions (Fig 6A and D). However, in Arpin knockdown hMDMs, there were still significantly more F-actin cups compared to control conditions albeit the global number had decreased (Fig 6D). We next calculated the enrichment of F-actin around internalised SRBC relative to the cell cortex. As expected, the enrichment of F-actin around internalised

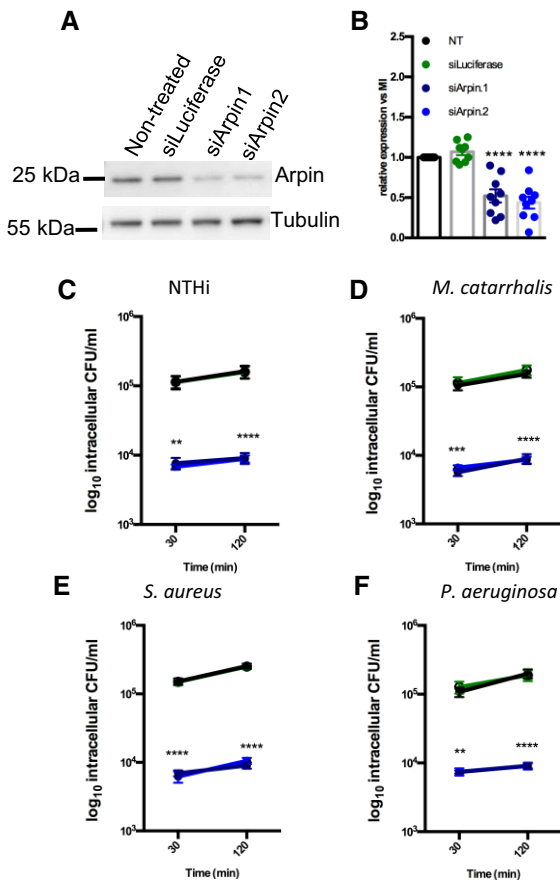


**Figure 5. Arpin knockdown impairs bacterial internalisation by macrophages.**

hMDMs were non-treated and treated with siLuciferase or 2 different Arpin siRNA sequences for 96 h

- A Immunoblot against Arpin and tubulin in siRNA-treated hMDMs.  
 B Quantification of the expression of Arpin normalised to tubulin and presented relative to non-treated as a percentage,  $n = 9$  donors, \*\*\*\* $P < 0.0001$  one-way ANOVA with Bonferroni's post-test vs. non-treated.  
 C–F (C) NTHi internalisation, (D) *Moraxella catarrhalis* internalisation, (E) *Staphylococcus aureus* internalisation and (F) *Pseudomonas aeruginosa* internalisation,  $n = 3$  donors, \*\*\* $P < 0.01$ , \*\*\*\* $P < 0.0001$ , \*\*\*\*\* $P < 0.00001$  two-way ANOVA with Dunnett's post-test vs. non-treated.

Data information: Error bars represent standard error of the mean (SEM). Source data are available online for this figure.

SRBC was similar for non-treated or siLuciferase-treated hMDMs at 15 min and decreased by 30 min (Fig 6E). Strikingly, in Arpin-depleted hMDMs, we observed significantly more F-actin enrichment around internalised SRBC at 15 and 30 min relative to control conditions (Fig 6E), consistent with the increased number of F-actin cups counted (Fig 6D). To better observe the membrane architecture when Arpin was knocked down in human macrophages, we performed scanning electron microscopy on Arpin siRNA or control siRNA-treated hMDMs after 15 min of internalisation of IgG-opsonised SRBC (Fig 6F). In control hMDMs, we could see a very thin covering of host membrane over the SRBC indicating near-complete internalisation (Fig 6F). In hMDMs treated with siRNA-targeting Arpin, we could observe accumulation of

membrane folds around the SRBC or thin membrane layers partially covering the particle (Fig 6F), which was reminiscent of the phenotype obtained after HRV16 treatment. This indicated that Arpin knockdown was impairing phagocytic cups progression and completion.

To further describe the role of Arpin in phagosome formation, we used the RAW264.7 murine cells transfected to transiently express lifeact-mCherry to detect polymerised branched actin and EGFP-Arpin. We performed the 3D phagosome formation and closure assay that we set up using total internal reflection fluorescence microscopy (TIRFM) [34,36,53,54] (Fig 6G and H). In this assay, living cells phagocytose particles that are non-covalently attached to the coverslips, allowing for observation of the base of the phagocytic cup in the epifluorescence mode when the stage is moved 3  $\mu\text{m}$  in  $z$ , the extending pseudopods, as well as the precise site of phagosome scission in the TIRFM mode (Fig 6G). We observed that Arpin was recruited at the site of phagosome formation with branched actin in the extending membrane folds (Fig 6H). The epifluorescence images showed that Arpin was not accumulated at the base of the phagosome in the region where actin is cleared. Interestingly, Arpin was enriched at the site of phagosome closure detected in both epifluorescence and TIRFM modes. Arpin is thus potentially playing a very local role in the actin polymerisation/depolymerisation cycle, rather than a role in the actin clearance at the base of the phagocytic cup.

Together, these results show that Arpin is not required for the initial onset of actin polymerisation but regulates the local branched actin network for a successful phagocytic cup extension and closure.

## Discussion

In this study, we show that HRV16 impairs the internalisation of bacteria and other particles by human macrophages. We reveal that Arpin is a host cell protein downregulated by the virus that is necessary and sufficient for the internalisation defect driven by HRV16 as re-expression rescued deficient internalisation in RPE-1 cells exposed to the virus. We further demonstrate for the first time that this Arp2/3 inhibitor is critical for efficient receptor-mediated phagocytosis and bacterial uptake in macrophages.

Our understanding of how macrophages, including differentiated tissue macrophages, deal with HRV infections compared to epithelial cells is incomplete [55]. There are reports indicating that HRV can infect monocytes/macrophages *in vitro* and *in vivo* [7,14,15,20,21,23]. In our work, we studied how differentiated human macrophages and resident lung-derived macrophages are affected by HRV infection. We first found that post-HRV16 exposure, macrophages did not internalise a range of gram-positive and gram-negative bacteria that are frequently associated with exacerbations [20]. Interestingly, we observed an innate impairment of bacterial internalisation in alveolar macrophages from healthy smokers compared to non-smoker controls that was further exacerbated following exposure to HRV16. The ability of smoking to worsen viral infections has been suggested, but the reports are still conflicting (for a review, see ref. [56]). Because reduced phagocytic capacities could be due to reduced surface phagocytic receptor expression [57], we explored whether bacterial binding to



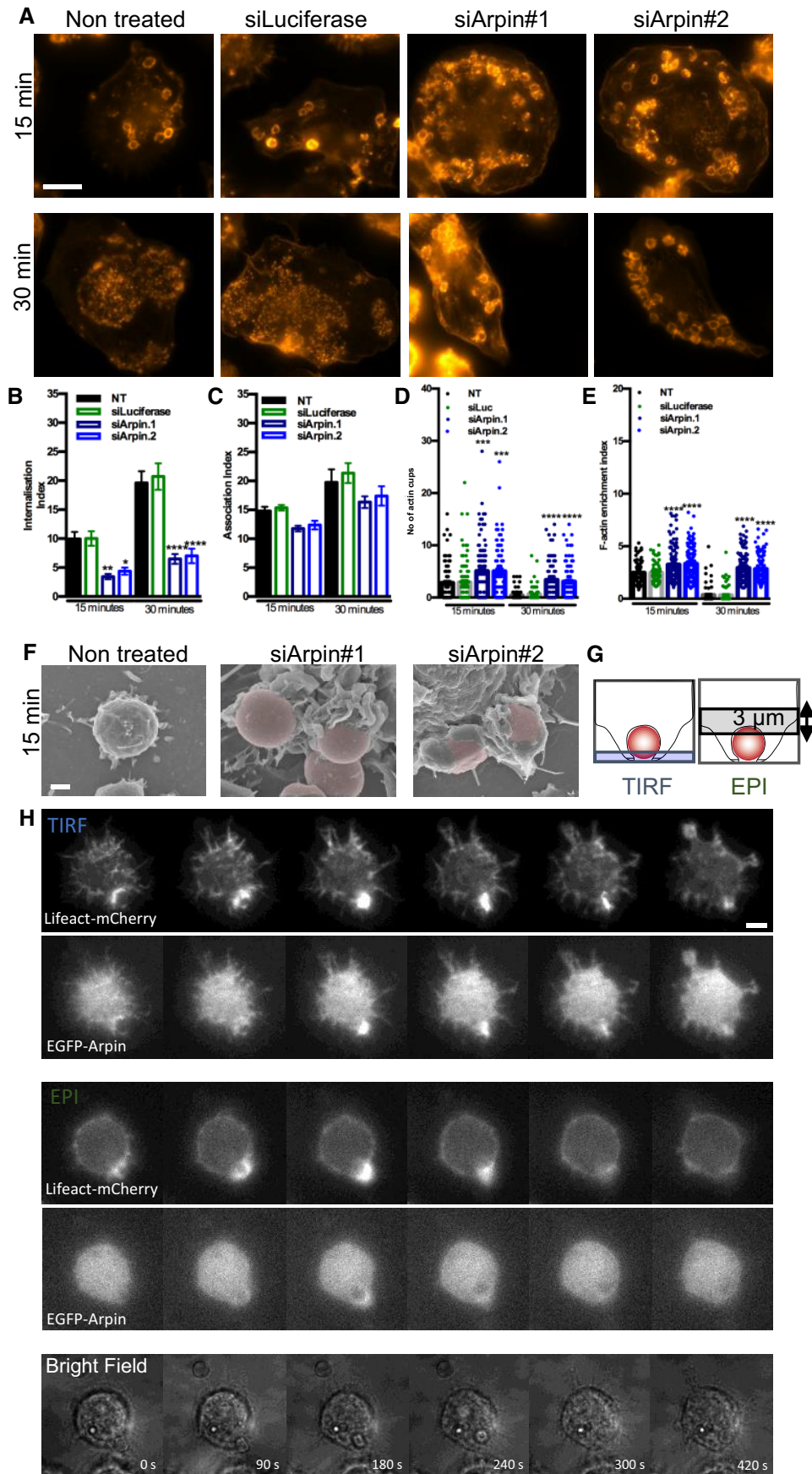


Figure 6.

**Figure 6. Arpin knockdown impairs efficient phagocytic cups formation and is recruited in membrane extensions and at the closure site.**

hMDMs were non-treated, treated with siLuciferase or two different Arpin siRNA sequences for 96 h, and then allowed to internalise IgG-opsonised SRBC for up to 30 min, and F-actin structures around phagocytosed particles were assessed using phalloidin-Cy3.

- A Representative images at 15 and 30 min post-internalisation. Scale bar, 15  $\mu$ m.
- B Quantification of internalisation of SRBC over 30 min,  $n = 3$  donors, 30 random cells/cover slip.
- C Quantification of association of SRBC to hMDMs over 30 min,  $n = 3$  donors, 30 random cells/cover slip.
- D Quantification of the number of F-actin cups in hMDMs over 30 min,  $n = 3$  donors, at least 60 cups in the early time point and between 15 and 60 depending on time point.
- E Quantification of the initial F-actin enrichment around internalised particles in hMDMs over 30 min,  $n = 3$  donors, at least 60 cups in the early time point and between 15 and 60 depending on time point.
- F Scanning electron microscopy images following Arpin knockdown or control and 15-min IgG-opsonised SRBC internalisation showing differences in membrane recruitment. Scale bar, 1  $\mu$ m.
- G Phagosome closure assay to detect the site of phagosome closure in the TIRFM mode (left) and the base of the phagosome in the epifluorescence mode after shifting the stage 3  $\mu$ m in z.
- H Phagosome closure assay was performed using RAW264.7 macrophages transiently expressing both Lifeact-mCherry and EGFP-Arpin. Lifeact-mCherry (upper panels) and EGFP-Arpin (lower panels) imaging by TIRFM and epifluorescence were performed alternatively at 37°C every 2 s for 10 min. Transmitted light images are presented at the bottom.

Data information: \* $P < 0.05$ , \*\* $P < 0.01$ , \*\*\* $P < 0.001$ , \*\*\*\* $P < 0.0001$  one-way ANOVA with Bonferroni's post-test vs. MI. Error bars represent standard error of the mean (SEM).

macrophages was affected. We found that this was not the case, further emphasising that HRV16 specifically affected the internalisation step. These results are important in the context of COPD where HRV is frequently isolated [20] and, together with other defective functions like cell activation [13,22–24], could be one of the explanations as to why patients show bacterial outgrowths post-HRV infection [13,19].

Phagocytosis is strictly dependent on actin polymerisation (for review, Refs. [26,58]), and upon phagocytosis, actin polymerisation at the site of particle binding is transient and intense and corresponds to the formation of a phagocytic cup. We demonstrate here that, although HRV16-challenged macrophages were impaired in internalisation over 30 min, they could form F-actin cups. However, there was an inherent delay to complete phagocytosis and to clear F-actin from forming phagosomes. Importantly, we were able to demonstrate that, while in mock-infected macrophages actin disassembled after 30 min, there was a maintenance of F-actin in phagocytic cups in HRV16-challenged macrophages. When we analysed the membrane extension over particles by scanning electron microscopy, we first observed that in contrast to monocytes [36], hMDMs seemed to have more folds of membrane around the particles. While there were multiple ruffles and folds of membrane in uninfected macrophages at 5 min, in HRV16-challenged macrophages, the membrane was a lot thinner and only partially covered the particle. In Arpin knockdown macrophages, we observed two phenotypes, either a very thin covering of membrane over the internalised particle, similar to HRV16, or small partial folds of membrane below the particle. All these results suggested that HRV16-challenged macrophages and Arpin-depleted macrophages show similar defects in their ability to promote actin remodelling and to extend membranes for efficient phagosome completion.

Arpin is a newly discovered inhibitor of the Arp2/3 complex that counteracts the activatory signals provided by the WAVE/Rac1 complex [45]. In addition to its reported role in cell steering and in controlling the lifetime of lamellipodia [45,49], it was shown to be dispensable for chemotactic migration of cancer cells and of *Dictyostelium discoideum* [59]. Of note, we found no significant difference in the spontaneous migration of macrophages between HRV-treated and control cells (Appendix Fig S1). As it has been documented that the Arp2/3 complex is critical for phagocytosis [60], and despite a

recent report [61], we postulated that the ability of Arpin to deactivate the Arp2/3 complex at sites of phagosome formation would also be important for efficient phagocytosis and that Arpin could play a role in this. Indeed, siRNA knockdown of Arpin impaired the internalisation of multiple bacteria as well as opsonised particles by macrophages without affecting their association. It has to be noted that the reduction in FcR-mediated phagocytosis measured in RPE-1 cells or in macrophages upon HRV16 treatment is lower than the reduction in initial uptake of bacteria after viral challenge. Other factors might be implicated in the virus-induced defective uptake of bacteria, in addition to Arpin. We found that Arpin was localised with branched actin in the extending membrane folds in the nascent phagosome, as well as at sites of phagosome scission, and not at the base of the phagosome where F-actin is cleared and where some other enzymatic activities like PLC or OCRL, involved in the actin depolymerisation, have been reported to be preferentially localised [36,38]. These results suggest that Arpin is playing a very local role in the actin polymerisation/depolymerisation cycle and regulation of the Arp2/3 complex, rather than a role in the actin clearance at the base of the phagocytic cup, which further expands our knowledge on the network of regulatory elements required for the dynamic actin remodelling and polymerisation/depolymerisation cycles that are necessary for efficient phagosome building by macrophages [26].

The Arpin protein level was decreased in HRV16-exposed human macrophages, which could be the consequence of different downregulation mechanisms. We analysed the mRNA levels of Arpin in HRV16-exposed hMDMs and there was a non-significant trend towards less expression also (Appendix Fig S2), indicating that HRV16 could affect Arpin expression at mRNA level in hMDMs. The virus could regulate transcription factors binding in the promoter region of the Arpin gene like NF- $\kappa$ B RelA, c-Rel and En1, as it has been shown for different promoters in HRV16-infected epithelial cells [62–64]. In addition, there could be miRNA regulation by the virus controlling mRNA stability and/or protein translation, as well as mechanisms of protein degradation. Interestingly, interrogation of public transcriptomic dataset [65] of alveolar macrophages from COPD smokers, healthy smokers and non-smokers revealed many genes differentially expressed in COPD smokers vs healthy smokers. Pathway analyses indicated a downregulation of the mechanisms of

actin polymerisation or cytoskeletal reorganisation, which further emphasises that actin regulation is key in COPD.

Our results demonstrate that Arpin is both necessary and sufficient for the impairment in internalisation driven by HRV16. This provides key insights into a major molecular player to explain how HRV16 is able to impair internalisation in hMDMs, which significantly builds on previous research [13]. Of note, the impairment of phagocytosis might be secondary to the establishment of viral factories hijacking cellular machineries and intracellular trafficking in the infected macrophages. In addition, the inhibition of bacterial uptake together with the inhibition of the cell inflammatory activity probably provides a beneficial environment for the virus itself.

In conclusion, our results demonstrate that Arpin is crucial for successful phagocytosis in macrophages and adds phagocytosis as a new function we can now attribute to this protein.

We reveal that Arpin is a major target of HRV16 infection, which opens new avenues for strategies to improve clearance of apoptotic cells and reduce inflammation and to increase bacterial uptake and suppress colonisation in the airways.

## Materials and Methods

### Antibodies and reagents

The following primary antibodies were used: mouse anti-actin (clone AC-40; Sigma, A3853), mouse anti-Cdc42 (BD Bioscience, 610929), mouse anti-Rac1 (BD Bioscience, 610650), rabbit anti-Arpin (kind gift from Alexis Gautreau), mouse anti-p16 (Synaptic Systems, 305011), rabbit anti-p34 (Merck Millipore, 07-227), rabbit anti-phospho cofilin (Cell Signalling #3313), mouse anti-total cofilin (Cell Signalling, Clone D3F9, #5175), mouse anti-tubulin alpha (clone DM1A, Sigma, T9026) and purified rabbit anti-SRBCs (IGN Biochemicals). DAPI was from Sigma (D9542) and phalloidin-Cy3 from Life Technologies (A22283). Zymosan A (Sigma-Aldrich) was coupled to Cy2 (GE Healthcare). Secondary antibodies were all from Jackson ImmunoResearch and were as follows: Cy5 or 488-labelled F(ab')<sub>2</sub> anti-rabbit IgG and mouse or rabbit anti-IgG-HRP. siRNA sequences were as follows: 5'-GGAGAA-CUGAUCGAUGUAUCU-3' (Arpin sequence 1) and 5'-GCUUCCUCAU-GUCGUCCUACA-3' (Arpin sequence 2), [45]. The control siRNA-targeting luciferase was 5'-CGUACGCGGAUACUUCGA-3'.

### Cell culture

Human peripheral blood mononuclear cells (PBMCs) were isolated from whole blood of healthy donors (Etablissement Français du Sang Ile-de-France, Site Trinité, Inserm agreement #15/EFS/012 and #18/EFS/030 ensuring that all donors gave a written informed consent and providing anonymised samples) by density gradient sedimentation using Ficoll-Paque (GE Healthcare). This was followed by adhesion on plastic at 37°C for 2 h and culture in the presence of adhesion medium (RPMI 1640 (Life Technologies) supplemented with 100 µg/ml streptomycin/penicillin and 2 mM L-glutamine (Invitrogen/Gibco)). Then, the adhered cells were washed once with warm adhesion medium and left to rest in macrophage medium (RPMI 1640 supplemented with 10% FCS (Eurobio), 100 µg/ml streptomycin/penicillin and 2 mM L-glutamine). On day 1, the cultures were washed with adhesion medium and then

supplemented every 2 days with fresh macrophage medium. The adherent monocytes were left to differentiate into macrophages as described previously [66] and used for experiments at day 10.

Human alveolar macrophages (AMs) were obtained by bronchoalveolar lavage fluid (BALF) of lung specimens from non-smokers or healthy smokers (Protocole de recherche non interventionnelle, Number ID RCB 2015-A01809) ensuring that all donors signed a consent form. The health condition of the patient was registered before the samples were treated anonymously. The sample was initially centrifuged at 290 g for 5 min, the pellet re-suspended in the original volume in adhesion medium, and the cell count obtained. Cells were then plated onto plastic and incubated for 4 h in adhesion medium at 37°C. They were then washed thoroughly with adhesion medium and rested overnight in AM media (X-VIVO 10 without phenol red and gentamicin (Lonza) supplemented with 50 µg/ml streptomycin/penicillin, 1 mM L-glutamine and 20 µg/ml amphotericin B (Sigma)), and experiments were performed the next day.

HeLa Ohio cells were purchased from the European Collection of Authenticated Cell Cultures (ECACC) and were cultured in DMEM GlutaMax containing 25 mM D-glucose and 1 mM sodium pyruvate (Life Technologies) supplemented with 10% FCS, 100 µg/ml penicillin/streptomycin and 2 mM L-glutamine. They were passaged every 3 days.

RAW264.7 macrophages were grown in complete medium, consisting of RPMI 1640 GlutaMAX supplemented with 10 mM HEPES, 1 mM sodium pyruvate, 50 µM beta-mercaptoethanol, 2 mM L-glutamine and 10% FCS (all from Gibco). Cells were transfected by electroporation with the Electrobuffer Kit (Cell project). Routinely, one 100-mm plate of cells was grown to subconfluence and 10 µg of each plasmid was used for co-transfections. The cells were electroporated in 0.4-cm cuvettes (Bio-Rad) at 250 V, 900 µF in an electroporation apparatus (X Pulser Bio-Rad Laboratories), then immediately re-suspended in complete culture medium. Efficiency of transfection was 10–40%.

### Generation of RPE-1-FcgRIIA cells

FcgRIIA gene was amplified by PCR from the pRK5-FcgRIIA plasmid (E. Caron, Imperial College, London) using the following oligos: forw: 5'-CCGGCGCCGCTCTCCAAGGTGTCC-3', and rev: 5'-GGCCCGACCGGTTTGTATTACTGTGACATGG-3' carrying respectively NotI and AgeI restriction site. The NotI/AgeI-digested amplicons were inserted in a pLEX MCS plasmid (Open Biosystems) digested as well and dephosphorylated. Lentiviral particles were produced by co-transfection of HEK293T cells with packaging plasmids (pCMV 8.91 and pEnv<sub>VSV-G</sub>) and pLEX-FcgRIIA plasmid. After 48 h of culture at 37°C, the virus-containing supernatant was filtered and ultracentrifuged at 60,000 g for 90 min at 4°C on a PEG cushion (50%). The virion-enriched pellet was re-suspended in PBS and aliquoted for storage at -80°C. hTERT RPE-1 cells (ATCC<sup>(R)</sup> no CRL-4000<sup>TM</sup>, BioPhenics facility, Institut Curie, Paris) were infected with lentiviral particles from MOI 1 to MOI 10. FcgRIIA-expressing hTERT RPE-1 cells were cultured in Dulbecco's modified Eagle's medium (DMEM) F-12 (Thermo Fisher Scientific) supplemented with 10% foetal calf serum (FCS, Gibco), 10 µg/ml hygromycin B and 2.5 µg/ml puromycin (Sigma). They were passaged every 2 days.

### RPE-1 cell transfection

RPE1 cells at 80% confluence were washed with PBS and detached using 0.25% Trypsin/EDTA (Life Technologies). After centrifugation, the cell count was determined and the cells were seeded on coverslips at a density of 15,000 per coverslip and allowed to adhere overnight. The next day, the coverslips were exposed to HRV16 or mock-infected as described above. Then, they were transferred to a 6-well plate and transfected. The plasmid solution was prepared in Opti-MEM medium (GlutaMAX supplemented, Gibco), containing FuGENE reagent (Invitrogen) and each plasmid at a concentration of 3 µg. Plasmid solution was added to each well and cultures left for 24 h at 37°C before being treated for FcR phagocytosis.

### Bacterial strains and culture

NTHi strain RdKW20 [67,68] and *Moraxella catarrhalis* strain 25293 [69] were purchased from the American Type Culture Collection (ATCC). *Staphylococcus aureus* strain 160201753001 and *Pseudomonas aeruginosa* strain 160601067201 from blood culture were provided by Professor Claire Poyart (Cochin Hospital). NTHi, *S. aureus* and *P. aeruginosa* were cultured on chocolate agar plates, and *M. catarrhalis* was cultured on brain-heart infusion (BHI) agar plates. Plates were incubated for 24 h at 37°C until colonies appeared. All strains were grown in LB medium, but for NTHi, this was also supplemented with 10 µg/ml hemin and 1 µg/ml nicotinamide adenine dinucleotide (NAD).

### Human rhinovirus production

Human rhinovirus 16 (HRV16) (VR-283, strain 11757, lot 62342987) was purchased from the ATCC, and stocks were produced by infecting HeLa Ohio cells in virus medium (DMEM GlutaMax containing 25 mM D-glucose and 1 mM sodium pyruvate supplemented with 10% FCS and 2 mM L-glutamine) as described previously [70]. Briefly, HeLa Ohio cells were grown to 80% confluence and infected with 5 ml HRV16 or control media for 1 h at room temperature with agitation. The remaining solution was made to 10 ml, and the cells with HRV16 left for 48 h to allow for 90% CPE to develop. Supernatants were then clarified by centrifugation and filtration [70], and 1 ml stocks were produced and stored at -80°C. To UV inactivate HRV16, it was treated with UV light (1,000 mJ/cm<sup>2</sup>) for 20 min. Inactivation was confirmed by adding the inactivated virus to HeLa Ohio cells and checking for CPE.

### Quantification of the tissue culture infective dose 50 (TCID<sub>50</sub>) of HRV16

HeLa Ohio cells were cultivated in 96-well plates at 1 × 10<sup>5</sup> cells/well for 24 h. HRV16 was diluted 10-fold from undiluted to 10<sup>-9</sup> in virus medium; 50 µl of each dilution was added to the cells in eight replicate wells. 50 µl of virus medium was added to two groups of control wells in eight replicate wells per group. Cultures were incubated for 4 days at 37°C until CPE was observed in 50% of wells. TCID<sub>50</sub> was calculated using the Spearman–Karber formula as previously outlined [70].

### HRV16 and bacterial infection of human macrophages

Macrophages were washed once in PBS and rested in virus medium. HRV16, HRV16<sup>UV</sup> or MI supernatants were added to the macrophages and placed at room temperature for 1 h with agitation to achieve a TCID<sub>50</sub> of 1 × 10<sup>7</sup>/ml. Cultures were then washed with virus medium and rested in macrophage medium overnight.

NTHi, *M. catarrhalis*, *S. aureus* or *P. aeruginosa* were grown until mid-log growth phase, centrifuged at 1,692 g for 5 min and re-suspended in 1 ml phagocytosis medium (RPMI supplemented with 2 mM L-glutamine). Bacteria were added to macrophages pre-treated with HRV16, HRV16<sup>UV</sup> or MI to achieve a multiplicity of infection (MOI) of 10/cell. Cultures were then centrifuged at 602 g for 2 min and placed at 37°C, 5% CO<sub>2</sub> for 30 or 120 min. At each time point, cultures were washed with PBS and treated with 100 µg/ml gentamicin (NTHi, *S. aureus*, *P. aeruginosa*) or 20 µg/ml (*M. catarrhalis*) for 20 min. Cultures were washed and lysed in saponin as previously described [66] and colony-forming units (CFU) estimated using the Miles–Misra technique [71].

### Measurement of bacterial binding

Macrophages were challenged with HRV16 or controls as described above, and bacteria were prepared in the same manner. Cultures were washed with PBS, and bacteria were added to macrophages to achieve an MOI of 10 bacteria per cell. They were placed on ice for 5, 15 or 30 min. At each time point, the extracellular supernatant was taken for CFU determination. Cultures were then washed with PBS and the final supernatant taken for CFU determination to verify that no residual bacteria remained. Cultures were then treated with saponin and lysed and CFU estimated as described previously [66].

### FcR, CR3 or zymosan phagocytosis

Macrophages were challenged with either IgM-ic3b- or IgG-opsonised SRBC or zymosan for up to 60 min as described [36]. Briefly, for CR3-mediated phagocytosis, SRBCs were washed in PBS/BSA 0.1% and incubated for 30 min with rotation in rabbit IgM anti-SRBCs. They were washed and incubated in complement C5-deficient serum without rotation for 20 min at 37°C. SRBCs were further washed, re-suspended in phagocytosis medium and added to macrophages to give approximately 10 SRBCs per cell. The plates were centrifuged at room temperature at 502 g for 2 min and then placed at 37°C for various time points. At each time point, cells were washed with room temperature phagocytosis medium and fixed in warm 4% paraformaldehyde (Sigma-Aldrich) at room temperature for 15 min and then treated with 0.05 M NH<sub>4</sub>Cl/PBS1X for 10 min. For FcR-mediated phagocytosis, SRBCs were washed as above and opsonised for 30 min with rotation in rabbit IgG anti-SRBCs. They were further washed, re-suspended in phagocytosis medium and added to macrophages as above. All subsequent steps were as for CR3. For zymosan uptake, zymosan was washed twice in PBS/BSA 0.1% and then re-suspended in phagocytosis medium. Macrophages were challenged with zymosan for 60 min, and all subsequent steps were as described above.



### Fluorescence Microscopy and phagocytosis quantification

For FcR- or CR3-mediated phagocytosis, cultures were washed in 1XPBS/2% FCS and external SRBCs were labelled for 30 min with F(ab')<sub>2</sub> anti-rabbit IgG Alexa Fluor 488 in PBS/2% FCS. Cells were then washed with 1XPBS/2%FCS and re-fixed in 4% PFA for 15 min at room temperature and then treated with 0.05 M NH<sub>4</sub>Cl for 10 min before being permeabilised in 1XPBS/2%FCS/0.05% saponin. Intracellular SRBCs were then detected using a Cy5-labelled F(ab')<sub>2</sub> anti-rabbit IgG, and F-actin was stained using phalloidin-Cy3 in 1XPBS/2%FCS/0.05% saponin for 30 min. After washing in 1XPBS/2%FCS/0.05% saponin, cells were stained with DAPI for 5 min and mounted using Fluoromount G (Interchim). For zymosan uptake, cultures were washed in 1XPBS/2% FCS and external zymosan was detected with an anti-zymosan antibody for 30 min followed by Cy5-labelled F(ab')<sub>2</sub> anti-rabbit IgG for 30 min. Cultures were washed in 1XPBS/2% FCS and permeabilised in 1XPBS/2%FCS/0.05% saponin before labelling with phalloidin Cy3 to detect F-actin. After washing as above, cultures were treated with DAPI for 5 min and mounted using Fluoromount G. To quantify phagocytosis, the number of internalised SRBCs/zymosan per cell was counted in 30 cells randomly chosen on the coverslips corresponding to the phagocytic index. The index obtained was divided by the index obtained for control cells and was expressed as a percentage of control cells. To determine the index of association, the total number of bound and internalised SRBCs in a cell was divided by the total number of macrophages counted. Image acquisition was performed on an inverted wide-field microscope (Leica DMI6000) with a 100× (1.4 NA) objective and a MicroMAX camera (Princeton Instruments). Z-series of images were taken at 0.3-µm increments. Analyses were performed using custom-made ImageJ (National Institutes of Health) routines.

### Quantification of F-actin recruitment in phagocytic cups and in macrophages

Quantification was performed as described previously [51]. Briefly, quantification was performed on ImageJ 64-bit software (NIH libraries) on a selected region in 1 plane of a 16-bit stack that was acquired. Primary fluorescence intensities through the phagocytic cup and in the cell cortex were measured and background-corrected. Ratio values were calculated by dividing the fluorescence intensities in the phagocytic cups by the fluorescence intensities in the cell cortex's and plotted. To quantify the F-actin intensity in HRV16-exposed macrophages, two macros were used. The first macro was written to quantify the intensity of staining in the entire field of cells. Quantification was performed using ImageJ 64-bit software on entire 16-bit Z stacks. The macro automatically decided which plane of the Z stack to use, and when in focus, it divided the field into four sections and quantified the fluorescence of the punctate F-actin and the total F-actin in each section. The second macro was written to quantify the intensity of the punctate F-actin per cell. This was done in the same way as for macro 1 apart from instead of calculating the intensity in the section, the macro quantified it in each individual cell within the field selected by the macro. To quantify the F-actin intensity, each macro used the

FindFocussedSlices filter and two automatic ImageJ thresholding. The first was percentile dark for the total F-actin, and the second was default dark for the punctate F-actin. The results from each output were reported as a summary for each cell or field in ImageJ. All results for both macros 1 and 2 were transferred to GraphPad Prism and plotted.

### Phagosome closure assay using total internal reflection fluorescence microscopy (TIRFM)

IgG-RBCs were centrifuged onto 35-mm glass bottom dishes (MatTek Corporation) pre-treated with 0.01% poly-L-lysine in PBS for 30 min at RT. The dishes were then washed once with a 10% BSA in PBS and incubated for 30 min with 10% BSA in PBS. Then, the dishes were incubated with pre-warmed serum-free microscopy medium. RAW264.7 macrophages were re-suspended and allowed to sediment onto opsonised SRBC-coated dishes at 37°C.

Total internal reflection fluorescence microscopy was performed using a Till PHOTONICS iMIC microscope equipped with an oil-immersion objective (Apo N 100×, NA1.49 Olympus America Inc.), a heating chamber and two cameras: a cooled iXonEM camera and an iXon3 897 Single Photon Detection EMCCD Camera (Andor Technology). The critical angle was verified at the beginning of each session by scanning through incident angles of 0–5° to maximise evanescent wave-induced fluorescence. Excitation was performed with a 491 nm and a 561 nm laser. For the phagosome closure assay, streams of 550 frames were acquired at 50 ms per frame in TIRF mode and 50 ms per frame in epifluorescence mode with polychrome illumination at a 3 µm increment every 2 s. TIRFM image streams were processed using ImageJ Color Profiler software (NIH).

### Migration assay

Human monocyte-derived macrophages were plated in IBIDI (15 µm) microscopy slides in eight wells, treated or not with the virus for 1 h, before washing and overnight rest in the incubator. They were then incubated with sirDNA at 0.33 µM and observed with a 20×, 1.4 NA, PH DIC objective with a spinning disc confocal (Yokogawa CSU-X1M1) inverted microscope (Leica DMI6000) equipped with a CoolSNAP HQ<sup>2</sup> camera (Photometrics) and a heated chamber with CO<sub>2</sub> in a BSL3 laboratory. Acquisition was performed with MetaMorph 7.5.5 (Molecular Devices) in the bright field (BF) and CY5 channel excited with a 635 nm laser.

### Western blots

Macrophages were lysed with lysis buffer (20 mM Tris-HCl, pH 7.5, 150 mM NaCl, 0.5% NP-40, 50 mM NaF and 1 mM sodium orthovanadate, supplemented with complete protease inhibitor cocktail (Roche Diagnostic)) for 15 min. Lysates were centrifuged at 16,100 g for 10 min at 4°C. The supernatants were removed and stored at -20 °C, and an equal concentration of protein (BCA dosage kit, Pierce) was analysed by SDS-PAGE. Proteins were transferred onto a polyvinylidene difluoride (PVDF) membrane (Millipore) at 4°C for 100 min and incubated in blocking solution

TBS/0.1% Tween-20 supplemented with 5% milk or BSA for 2 h. Blots were rinsed with TBS/0.1% Tween-20, and primary antibodies were incubated in the blocking solution overnight or for 2 h as required. The membrane was further washed and incubated with HRP-coupled secondary antibodies in blocking buffer for 45 min. Detection was performed using ECL Dura substrate (GE Healthcare), and bands were imaged by Fusion (Vilber Lourmat) and quantified in ImageJ.

### Scanning electron microscopy

Cells were fixed with 2.5% glutaraldehyde (Sigma-Aldrich) in 0.1 M HEPES, pH 7.2 in phagocytosis medium at 37°C for 1 h. They were then fixed in 2.5% glutaraldehyde in 0.1 M HEPES buffer in PBS at 4°C overnight. Post-fixation was done with 1% osmium tetroxide (Merck) and 1.5% ferrocyanide (Sigma-Aldrich) in 0.1 M HEPES. After dehydration by a graded series of ethanol, the samples were transferred to a Leica EM CPD300 and dried according to standard procedures. Samples were mounted on aluminium stubs and sputter-coated with 7 nm of gold-palladium in a Gatan ion beam coater. Samples were examined at 5 kV in an JEOL 6700F scanning electron microscope.

### siRNA treatment

Macrophages at day 7 were washed twice with macrophage medium and kept in macrophage medium at 37°C. The siRNA solution was prepared in Opti-MEM medium (GlutaMAX supplemented, Gibco), containing Lipofectamine RNAiMAX reagent (Invitrogen) and siRNA at a concentration of 100  $\mu$ M. siRNA was added to each well and cultures left for 96 h at 37°C before being used. siRNA sequences were as follows: CGU ACG CGG AAU ACU UCG A55 (siLuciferase\_pGL2), GGA GAA CUG AUC GAU GUA UCU 55 (siArpin.1) and GCU UCC UCA UGU CGU CCU ACA 55 (siArpin.2).

### qPCR

Human monocyte-derived macrophages were exposed to HRV16 or MI control as described above. After overnight rest, cultures were washed with PBS and RNA was extracted as previously described [72]. Briefly, hMDMs were washed with PBS at room temperature and lysed using TRIzol reagent (Thermo Fisher Scientific). Proteins (organic phase) and RNA and DNA (aqueous phase) were separated using chloroform for 2 min at room temperature followed by 15-min centrifugation at 4°C at 12,000 g. The aqueous phase was collected, and isopropanol was added to precipitate RNA and incubated for 10 min at room temperature. Samples were centrifuged for 20 min at 4°C at 15,000 g and the pellet of RNA washed with 75% ethanol and centrifuged for a further 5 min at 4°C at 10,000 g. The pellet was dried at room temperature and re-suspended in pure water and warmed at 55°C for 5 min. The total amount of RNA was quantified using NanoDrop. For reverse transcription, 1  $\mu$ g of mRNA was retro-transcribed into DNA using SuperScript II Reverse Transcriptase (Thermo Fisher Scientific). qPCR was performed using the LightCycler 480 SYBR Green I Master (Roche) with specific oligos to detect Arpin with 18S RNA as control (Table 2). The relative quantification of Arpin gene expression was assessed using the  $\Delta\Delta C_t$  method [73].

**Table 2.** List of qPCR primers used in this study.

Gene	Sequence	References
18S histone	Forward: AGGAATTGACGGAAGGGCAC	[74]
	Reverse: GGACATCTAAGGGCATCACA	
Arpin	Forward: CTTCTCATGTCTGCTCTACAAGGTG	[45]
	Reverse: CTGTCAGCGCGAGCAGCTCT	

### Statistical analysis

Statistical tests were performed using GraphPad prism® version 6 software. All statistical tests are listed in the figure legends, and significance was determined if  $P < 0.05$ .

**Expanded View** for this article is available online.

### Acknowledgements

The team thanks Alexis Gautreau for insights into the work and for providing us with reagents related to Arpin. We thank the entire pneumology department at the Hospital Cochin for their help in acquiring BAL samples necessary for this study. We also thank Maryse Moya-Nilges at Institut Pasteur Paris, Paris, for help in preparing and analysing the scanning electron microscopy data. Thanks are also extended to Claire Poyart for bacterial strains, Lisa Parker for help with calculating rhinovirus TCID<sub>50</sub>'s and summer students who participated in some experiments: Ferran Colomies, Thomas Di Costanzo and Aurélie Masson. Work in the FN laboratory was supported by CNRS, Inserm, Université Paris Descartes and a collaborative grant with AstraZeneca.

### Author contributions

Conceptualisation: JJ, NK and FN. Methodology: JJ, FH, EI, LO, PB and FN. Investigation: JJ, KA-G, FH, AM and PB. Resources: PB and P-RB. Writing: original draft: JJ, KA-G, FH and FN. Writing: review and editing: GM, DMC, NK and FN. Supervision: NK and FN. Project administration: GM, DMC, NK and FN. Funding acquisition: GM, DMC, NK and FN.

### Conflict of interest

NK, DMC, LO, EI and GM are employed by the commercial company AstraZeneca, and AstraZeneca provided salaries for JJ and KAG as part of a collaborative grant with FN. All authors have no conflict of interest to declare.

### References

- Jacobs SE, Lamson DM, St George K, Walsh TJ (2013) Human rhinoviruses. *Clin Microbiol Rev* 26: 135–162
- Staunton DE, Merluzzi VJ, Rothlein R, Barton R, Marlin SD, Springer TA (1989) A cell adhesion molecule, ICAM-1, is the major surface receptor for rhinoviruses. *Cell* 56: 849–853
- Hofer F, Gruenberger M, Kowalski H, Machat H, Huettinger M, Kuechler E, Blaas D (1994) Members of the low density lipoprotein receptor family mediate cell entry of a minor-group common cold virus. *Proc Natl Acad Sci USA* 91: 1839–1842
- Palmenberg AC, Spiro D, Kuzmickas R, Wang S, Djikeng A, Rathe JA, Fraser-Liggett CM, Liggett SB (2009) Sequencing and analyses of all known human rhinovirus genomes reveal structure and evolution. *Science* 324: 55–59

5. Bochkov YA, Watters K, Ashraf S, Griggs TF, Devries MK, Jackson DJ, Palmenberg AC, Gern JE (2015) Cadherin-related family member 3, a childhood asthma susceptibility gene product, mediates rhinovirus C binding and replication. *Proc Natl Acad Sci USA* 112: 5485–5490
6. Arruda E, Boyle TR, Winther B, Pevear DC, Gwaltney JM Jr, Hayden FG (1995) Localization of human rhinovirus replication in the upper respiratory tract by *in situ* hybridization. *J Infect Dis* 171: 1329–1333
7. Gern JE, Dick EC, Lee WM, Murray S, Meyer K, Handzel ZT, Busse WW (1996) Rhinovirus enters but does not replicate inside monocytes and airway macrophages. *J Immunol* 156: 621–627
8. api A, Johnston SL (1999) Rhinovirus infection induces expression of its own receptor intercellular adhesion molecule 1 (ICAM-1) via increased NF-kappaB-mediated transcription. *J Biol Chem* 274: 9707–9720
9. Winther B, Arruda E, Witek TJ, Marlin SD, Tsianco MM, Innes DJ, Hayden FG (2002) Expression of ICAM-1 in nasal epithelium and levels of soluble ICAM-1 in nasal lavage fluid during human experimental rhinovirus infection. *Arch Otolaryngol Head Neck Surg* 128: 131–136
10. Whiteman SC, Bianco A, Knight RA, Spiteri MA (2003) Human rhinovirus selectively modulates membranous and soluble forms of its intercellular adhesion molecule-1 (ICAM-1) receptor to promote epithelial cell infectivity. *J Biol Chem* 278: 11954–11961
11. Sajjan U, Wang Q, Zhao Y, Gruenert DC, Hershenson MB (2008) Rhinovirus disrupts the barrier function of polarized airway epithelial cells. *Am J Respir Crit Care Med* 178: 1271–1281
12. Kennedy JL, Turner RB, Braciale T, Heymann PW, Borish L (2012) Pathogenesis of rhinovirus infection. *Curr Opin Virol* 2: 287–293
13. Oliver BG, Lim S, Wark P, Laza-Stanca V, King N, Black JL, Burgess JK, Roth M, Johnston SL (2008) Rhinovirus exposure impairs immune responses to bacterial products in human alveolar macrophages. *Thorax* 63: 519–525
14. Laza-Stanca V, Stanciu LA, Message SD, Edwards MR, Gern JE, Johnston SL (2006) Rhinovirus replication in human macrophages induces NF-kappaB-dependent tumor necrosis factor alpha production. *J Virol* 80: 8248–8258
15. Zhou X, Zhu L, Lizarraga R, Chen Y (2017) Human airway epithelial cells direct significant rhinovirus replication in monocytic cells by enhancing ICAM1 expression. *Am J Respir Cell Mol Biol* 57: 216–225
16. Blaas D, Fuchs R (2016) Mechanism of human rhinovirus infections. *Mol Cell Pediatr* 3: 21
17. Gern JE, Galagan DM, Jarjour NN, Dick EC, Busse WW (1997) Detection of rhinovirus RNA in lower airway cells during experimentally induced infection. *Am J Respir Crit Care Med* 155: 1159–1161
18. Papadopoulos NG, Papi A, Meyer J, Stanciu LA, Salvi S, Holgate ST, Johnston SL (2001) Rhinovirus infection up-regulates eotaxin and eotaxin-2 expression in bronchial epithelial cells. *Clin Exp Allergy* 31: 1060–1066
19. Wilkinson TM, Hurst JR, Perera WR, Wilks M, Donaldson GC, Wedzicha JA (2006) Effect of interactions between lower airway bacterial and rhinoviral infection in exacerbations of COPD. *Chest* 129: 317–324
20. Wilkinson TMA, Aris E, Bourne S, Clarke SC, Peeters M, Pascal TG, Schoonbroodt S, Tuck AC, Kim V, Ostridge K et al (2017) A prospective, observational cohort study of the seasonal dynamics of airway pathogens in the aetiology of exacerbations in COPD. *Thorax* 72: 919–927
21. Bentley JK, Sajjan US, Dzaman MB, Jarjour NN, Lee WM, Gern JE, Hershenson MB (2013) Rhinovirus colocalizes with CD68- and CD11b-positive macrophages following experimental infection in humans. *J Allergy Clin Immunol* 132: 758–761.e3
22. Unger BL, Faris AN, Ganesan S, Comstock AT, Hershenson MB, Sajjan US (2012) Rhinovirus attenuates non-typeable Hemophilus influenzae-stimulated IL-8 responses via TLR2-dependent degradation of IRAK-1. *PLoS Pathog* 8: e1002969
23. Finney LJ, Belchamber KBR, Fenwick PS, Kemp SV, Edwards MR, Mallia P, Donaldson G, Johnston SL, Donnelly LE, Wedzicha JA (2019) Human rhinovirus impairs the innate immune response to bacteria in alveolar macrophages in chronic obstructive pulmonary disease. *Am J Respir Crit Care Med* 199: 1496–1507
24. Jubrail J, Africano-Gomez K, Herit F, Baturcam E, Mayer E, Mootoosamy Cunoosamy D, Kurian N, Niedergang F (2018) HRV16 impairs macrophages cytokine response to a secondary bacterial trigger. *Front Immunol* 9: 2908
25. Niedergang F (2016) Phagocytosis. In *Encyclopedia of Cell Biology*, Bradshaw R, Stahl P (eds), pp 751–757. Waltham, MA: Academic Press
26. Niedergang F, Grinstein S (2018) How to build a phagosome: new concepts for an old process. *Curr Opin Cell Biol* 50: 57–63
27. Flannagan RS, Cosio G, Grinstein S (2009) Antimicrobial mechanisms of phagocytes and bacterial evasion strategies. *Nat Rev Microbiol* 7: 355–366
28. Flannagan RS, Jaumouille V, Grinstein S (2012) The cell biology of phagocytosis. *Annu Rev Pathol* 7: 61–98
29. Canton J, Neculai D, Grinstein S (2013) Scavenger receptors in homeostasis and immunity. *Nat Rev Immunol* 13: 621–634
30. Caron E, Hall A (1998) Identification of two distinct mechanisms of phagocytosis controlled by different Rho GTPases. *Science* 282: 1717–1721
31. Niedergang F, Chavrier P (2005) Regulation of phagocytosis by Rho GTPases. *Curr Top Microbiol Immunol* 291: 43–60
32. Swanson JA (2008) Shaping cups into phagosomes and macropinosomes. *Nat Rev Mol Cell Biol* 9: 639–649
33. Hoppe AD, Swanson JA (2004) Cdc42, Rac1, and Rac2 display distinct patterns of activation during phagocytosis. *Mol Biol Cell* 15: 3509–3519
34. Marie-Anais F, Mazzolini J, Herit F, Niedergang F (2016) Dynamin-actin cross talk contributes to phagosome formation and closure. *Traffic* 17: 487–499
35. Greenberg S, el Khoury J, di Virgilio F, Kaplan EM, Silverstein SC (1991) Ca<sup>2+</sup>-independent F-actin assembly and disassembly during Fc receptor-mediated phagocytosis in mouse macrophages. *J Cell Biol* 113: 757–767
36. Marion S, Mazzolini J, Herit F, Bourdoncle P, Kambou-Pene N, Hailfinger S, Sachse M, Ruland J, Benmerah A, Echard A et al (2012) The NF-kappaB signaling protein Bcl10 regulates actin dynamics by controlling AP1 and OCRL-bearing vesicles. *Dev Cell* 23: 954–967
37. May RC, Machesky LM (2001) Phagocytosis and the actin cytoskeleton. *J Cell Sci* 114: 1061–1077
38. Schlam D, Bagshaw RD, Freeman SA, Collins RF, Pawson T, Fairn GD, Grinstein S (2015) Phosphoinositide 3-kinase enables phagocytosis of large particles by terminating actin assembly through Rac/Cdc42 GTPase-activating proteins. *Nat Commun* 6: 8623
39. Araki N, Johnson MT, Swanson JA (1996) A role for phosphoinositide 3-kinase in the completion of macropinocytosis and phagocytosis by macrophages. *J Cell Biol* 135: 1249–1260
40. Bohdanowicz M, Balkin DM, De Camilli P, Grinstein S (2012) Recruitment of OCRL and Inpp5B to phagosomes by Rab5 and APPL1 depletes phosphoinositides and attenuates Akt signaling. *Mol Biol Cell* 23: 176–187

41. Cox D, Tseng CC, Bjekic G, Greenberg S (1999) A requirement for phosphatidylinositol 3-kinase in pseudopod extension. *J Biol Chem* 274: 1240–1247
42. Ulvila J, Vanha-aho LM, Kleino A, Vaha-Makila M, Vuoksio M, Eskelinen S, Hultmark D, Kocks C, Hallman M, Parikka M et al (2011) Cofilin regulator 14-3-3zeta is an evolutionarily conserved protein required for phagocytosis and microbial resistance. *J Leukoc Biol* 89: 649–659
43. Maritzen T, Zech T, Schmidt MR, Krause E, Machesky LM, Haucke V (2012) Gadin negatively regulates cell spreading and motility via sequestration of the actin-nucleating ARP2/3 complex. *Proc Natl Acad Sci USA* 109: 10382–10387
44. Rocca DL, Martin S, Jenkins EL, Hanley JG (2008) Inhibition of Arp2/3-mediated actin polymerization by PICK1 regulates neuronal morphology and AMPA receptor endocytosis. *Nat Cell Biol* 10: 259–271
45. Dang I, Gorelik R, Sousa-Blin C, Derivery E, Guerin C, Linkner J, Nemethova M, Dumortier JG, Giger FA, Chipysheva TA et al (2013) Inhibitory signalling to the Arp2/3 complex steers cell migration. *Nature* 503: 281–284
46. Molinie N, Gautreau A (2018) The Arp2/3 regulatory system and its deregulation in cancer. *Physiol Rev* 98: 215–238
47. Fetis S, Thureau A, Campanacci V, Aumont-Nicaise M, Dang I, Gautreau A, Perez J, Cherfils J (2016) Hybrid structural analysis of the Arp2/3 regulator arpin identifies its acidic tail as a primary binding epitope. *Structure* 24: 252–260
48. Sokolova OS, Chemeris A, Guo S, Alioto SL, Gandhi M, Padrick S, Pechnikova E, David V, Gautreau A, Goode BL (2017) Structural basis of Arp2/3 complex inhibition by GMF, coronin, and arpin. *J Mol Biol* 429: 237–248
49. Gorelik R, Gautreau A (2015) The Arp2/3 inhibitory protein arpin induces cell turning by pausing cell migration. *Cytoskeleton (Hoboken)* 72: 362–371
50. Caramori G, Adcock I (2003) Pharmacology of airway inflammation in asthma and COPD. *Pulm Pharmacol Ther* 16: 247–277
51. Braun V, Deschamps C, Raposo G, Benaroch P, Benmerah A, Chavrier P, Niedergang F (2007) AP-1 and ARF1 control endosomal dynamics at sites of FcR mediated phagocytosis. *Mol Biol Cell* 18: 4921–4931
52. Eden S, Rohatgi R, Podtelebnikov AV, Mann M, Kirschner MW (2002) Mechanism of regulation of WAVE1-induced actin nucleation by Rac1 and Nck. *Nature* 418: 790–793
53. Marie-Anais F, Mazzolini J, Bourdoncle P, Niedergang F (2016) “Phagosome Closure Assay” to visualize phagosome formation in three dimensions using total internal reflection fluorescent microscopy (TIRFM). *J Vis Exp* <https://doi.org/10.3791/54470>
54. Mularski A, Marie-Anais F, Mazzolini J, Niedergang F (2018) Observing frustrated phagocytosis and phagosome formation and closure using total internal reflection fluorescence microscopy (TIRFM). *Methods Mol Biol* 1784: 165–175
55. Cole J, Aberdein J, Jubrail J, Dockrell DH (2014) The role of macrophages in the innate immune response to *Streptococcus pneumoniae* and *Staphylococcus aureus*: mechanisms and contrasts. *Adv Microb Physiol* 65: 125–202
56. Jubrail J, Kurian N, Niedergang F (2017) Macrophage phagocytosis cracking the defect code in COPD. *Biomed J* 40: 305–312
57. Hodge S, Hodge G, Ahern J, Jersmann H, Holmes M, Reynolds PN (2007) Smoking alters alveolar macrophage recognition and phagocytic ability: implications in chronic obstructive pulmonary disease. *Am J Respir Cell Mol Biol* 37: 748–755
58. Freeman SA, Grinstein S (2014) Phagocytosis: receptors, signal integration, and the cytoskeleton. *Immunol Rev* 262: 193–215
59. Dang I, Linkner J, Yan J, Irimia D, Faix J, Gautreau A (2017) The Arp2/3 inhibitory protein Arpin is dispensable for chemotaxis. *Biol Cell* 109: 162–166
60. May RC, Caron E, Hall A, Machesky LM (2000) Involvement of the Arp2/3 complex in phagocytosis mediated by Fcγ<sub>3</sub> or CR5. *Nat Cell Biol* 2: 246–248
61. Rotty JD, Brighton HE, Craig SL, Asokan SB, Cheng N, Ting JP, Bear JE (2017) Arp2/3 complex is required for macrophage integrin functions but is dispensable for FcR phagocytosis and *in vivo* motility. *Dev Cell* 42: 498–513.e6
62. Hudy MH, Traves SL, Proud D (2014) Transcriptional and epigenetic modulation of human rhinovirus-induced CXCL10 production by cigarette smoke. *Am J Respir Cell Mol Biol* 50: 571–582
63. Hudy MH, Traves SL, Wiehler S, Proud D (2010) Cigarette smoke modulates rhinovirus-induced airway epithelial cell chemokine production. *Eur Respir J* 35: 1256–1263
64. Maciejewski BA, Jamieson KC, Arnason JW, Kooi C, Wiehler S, Traves SL, Leigh R, Proud D (2017) Rhinovirus-bacteria coexposure synergistically induces CCL20 production from human bronchial epithelial cells. *Am J Physiol Lung Cell Mol Physiol* 312: L731–L740
65. Shaykhiev R, Krause A, Salit J, Strulovici-Barel Y, Harvey BG, O'Connor TP, Crystal RG (2009) Smoking-dependent reprogramming of alveolar macrophage polarization: implication for pathogenesis of chronic obstructive pulmonary disease. *J Immunol* 183: 2867–2883
66. Jubrail J, Morris P, Bewley MA, Stoneham S, Johnston SA, Foster SJ, Peden AA, Read RC, Marriott HM, Dockrell DH (2016) Inability to sustain intraphagolysosomal killing of *Staphylococcus aureus* predisposes to bacterial persistence in macrophages. *Cell Microbiol* 18: 80–96
67. Bishop-Hurley SL, Schmidt FJ, Erwin AL, Smith AL (2005) Peptides selected for binding to a virulent strain of *Haemophilus influenzae* by phage display are bactericidal. *Antimicrob Agents Chemother* 49: 2972–2978
68. Domenech M, Pedrero-Vega E, Prieto A, Garcia E (2016) Evidence of the presence of nucleic acids and beta-glucan in the matrix of non-typeable *Haemophilus influenzae in vitro* biofilms. *Sci Rep* 6: 36424
69. Blakeway LV, Power PM, Jen FE, Worboys SR, Boitano M, Clark TA, Korlach J, Bakaletz LO, Jennings MP, Peak IR et al (2014) ModM DNA methyltransferase methylome analysis reveals a potential role for *Moraxella catarrhalis* phasevarions in otitis media. *FASEB J* 28: 5197–5207
70. Bennett JA, Prince LR, Parker LC, Stokes CA, de Bruin HG, van den Berge M, Heijink IH, Whyte MK, Sabroe I (2012) Pellino-1 selectively regulates epithelial cell responses to rhinovirus. *J Virol* 86: 6595–6604
71. Miles AA, Misra SS, Irwin JO (1938) The estimation of the bactericidal power of the blood. *J Hyg (Lond)* 38: 732–749
72. Chomczynski P, Sacchi N (1987) Single-step method of RNA isolation by acid guanidinium thiocyanate-phenol-chloroform extraction. *Anal Biochem* 162: 156–159
73. Livak KJ, Schmittgen TD (2001) Analysis of relative gene expression data using real-time quantitative PCR and the 2<sup>-ΔΔC<sub>T</sub></sup> Method. *Methods* 25: 402–408
74. Génin P, Cuvelier F, Lambin S, Côte-Real Filipe J, Autrusseau E, Laurent C, Laplantine E, Weil R (2015) Correction: Optineurin regulates the interferon response in a cell cycle-dependent manner. *PLoS Pathog* 11: e1004971